technologies

MDPI

Letter

Facile Fabrication of Macroscopic Self-Standing Ni or Co-doped MnO_2 Architectures as Catalysts for Propane Oxidation

Long Chen [1,2] and Xiping Song [1,*]

[1] State Key Laboratory for Advanced Metals and Materials, University of Science and Technology Beijing, Beijing 100083, China; clong1113@gmail.com

[2] Beijing Institute of Metrology, Beijing 100029, China

* Correspondence: xpsong@skl.ustb.edu.cn; Tel.: +86-10-6233-3213

Received: 17 October 2019; Accepted: 8 November 2019; Published: 11 November 2019

Abstract: The fabrication of macroscopic self-standing architectures plays a key role in the practical applications of nanomaterials. A facile strategy to assemble MnO_2 nanowires into macroscopic self-standing architectures via hydrothermal reaction followed by ambient pressure drying was developed. The obtained sample was robust and showed excellent mechanical strength with a Young's modulus of 127 MPa, which had the possibility for practical applications. In order to promote the catalytic activity for propane oxidation, Ni or Co doping into MnO_2 was studied. The results showed that the obtained macroscopic self-standing Ni-MnO_2 and Co-MnO_2 architectures exhibited enhanced catalytic activities for propane oxidation. Specifically, the conversions of propane over Co-MnO_2 and Ni-MnO_2 samples at 400 °C were 27.3% and 25.7% higher than that over pristine MnO_2 sample.

Keywords: macroscopic self-standing architectures; Ni-doped MnO_2; Co-doped MnO_2; propane oxidation; mechanical properties

1. Introduction

Amongst various transition metal oxides, manganese dioxide has been considered as one of the most potential low-temperature catalysts due to its environmental friendliness as well as its low cost [1]. In order to further improve the catalytic activity of MnO_2, one of the most common strategies is doping with a different cation, such as Ni [2,3] and Co [4,5]. On the other hand, self-assembly of nanomaterials into macroscopic architectures provides the possibility for exploring the practical applications. However, the method to assemble nanomaterials into macroscopic architectures remains a challenge [6,7].

Long et al. [8] obtained a macro-assembly with MnO_2 nanowires via a hydrothermal method followed by a freeze-drying process, which showed selective adsorption of cationic dyes. Jung et al. [9] constructed MnO_2 nanowire hydrogel/aerogels via hydrothermal synthesis (over four days) and supercritical drying, which could be used to remove heavy metal ions and toxic organic contents in water. Suib et al. [10] constructed macroscopic free-standing OMS-2 sponges through hydrothermal reaction (250 °C for four days) and freeze-drying process, which could be used to separate oil and water. Rong et al. [11] fabricated a three-dimensional manganese dioxide framework combining δ-MnO_2 nanosheets and α-MnO_2 nanowires, which had interconnected network structures and showed excellent oxidation activity for ppm-level HCHO to CO_2 at low temperatures (≤120 °C). However, the reported process was time-consuming and high cost, and the catalytic application at higher temperature was rarely concerned. Therefore, it is necessary to explore simpler preparation methods and study the catalytic performance at higher reaction temperatures.

This research aims to fabricate macroscopic self-standing architectures with metal doped MnO_2 nanomaterials via facile hydrothermal reaction followed by ambient pressure drying and study the catalytic activity for propane oxidation. To the best of our knowledge, the study of macroscopic architectures with metal doped MnO_2 nanowires as catalysts for propane oxidation has been scarcely reported.

2. Materials and Methods

The macroscopic self-standing MnO_2 architectures were prepared by a modified hydrothermal process followed by ambient pressure drying. Typically, the A aqueous solution consisting of manganese acetate ($Mn(CH_3COO)_2{\cdot}4H_2O$, 1.18 g) and ammonium sulfate ($(NH_4)_2SO_4$, 3 g) was added slowly into the B aqueous solution consisting of potassium permanganate ($KMnO_4$, 0.506 g) and cetyl trimethylammonium bromide ($C_{19}H_{42}BrN$, 0.09 g) with continuous stirring. Afterwards, the resultant slurry was treated under hydrothermal conditions at 140 °C and kept for 6 h. Then the produced wet gel was washed in distilled water at 50 °C repeatedly. After ambient pressure drying, the macroscopic free-standing MnO_2 with the specific shape of the drying vessel was obtained. The schematic diagram of the preparation process for macroscopic self-standing architectures was shown in Figure 1.

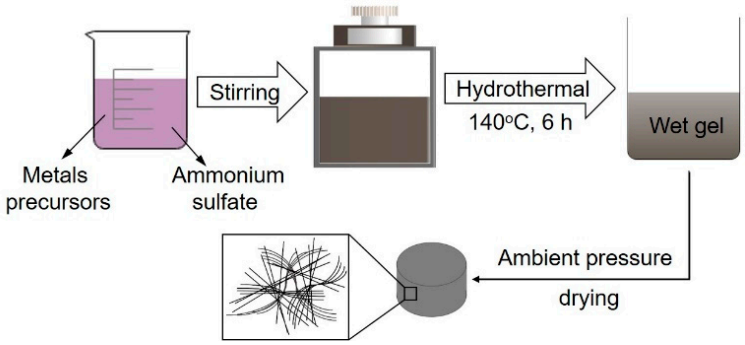

Figure 1. The schematic diagram of the preparation process for macroscopic self-standing architectures.

The macroscopic self-standing Ni- or Co-doped MnO_2 architectures were prepared by a similar procedure including the addition of nickel nitrate or cobalt nitrate precursors. The doping amounts of Ni (Ni/Mn molar ratio of 3/5) or Co (Co/Mn molar ratio of 1/5) were optimized in previous research [12,13] and the obtained samples were designated as Ni-MnO_2 and Co-MnO_2, respectively.

An X-ray diffractometer (XRD, D8 Advance A25, Bruker, Germany) was employed to identify the phase structure. The morphologies were investigated with Scanning Electron Microscopy (SEM, SUPRATM 55, Carl Zeiss, Germany). An Instron 5940 universal testing machine (Shanghai, China) was employed for compression testing of pristine MnO_2, Ni- or Co-doped MnO_2 samples.

The catalytic activities of propane oxidation over pristine MnO_2, Ni- or Co-doped MnO_2 samples were evaluated in a fixed-bed reactor with continuous flow. The feed gas consisted of 1000 ppm propane, 5% oxygen in a nitrogen balance gas, and total flow rate was 300 mL/min. A mixture of 0.4 g sample and quartz sands was used, and the heating rate of the oxidation reaction was 5 °C/min. The maximum pressure reached inside the reactor was 103 kPa. The propane concentration in the outlet gas was on-line monitored with a MultiGas analyzer (MKS MultiGas ™ 2030, USA). The propane conversion was defined according to the following equation:

$$\text{Propane conversion (\%)} = (1 - [C_3H_8]_{outlet}/[C_3H_8]_{inlet}) \times 100\%, \quad (1)$$

3. Results and Discussion

The appearance of prepared macroscopic self-standing MnO_2 architectures with cylindrical shapes was shown in the inset of Figure 2. The appearance of Ni-MnO_2 and Co-MnO_2 were similar to that of MnO_2. It demonstrates that the Ni or Co doping did not interrupt the assembling process of

macroscopic self-standing MnO_2 architectures. The XRD patterns (Figure 1) suggested that the crystal phases of pristine MnO_2, Ni-MnO_2 and Co-MnO_2 samples corresponded well to the tetragonal MnO_2 (JCPDS no. 44-0141). No impurity phase was observed, which validated the high dispersion state of Ni or Co within the MnO_2 framework. The statistical average bulk densities of MnO_2, Ni-MnO_2 and Co-MnO_2 samples were 0.72, 0.69 and 0.70 g cm^{-3}, respectively. The morphologies of pristine MnO_2, Ni-MnO_2 and Co-MnO_2 samples were shown in Figure 3. The basic component unit of pristine MnO_2 was nanowire, with a length of several hundred micrometers. The bundles of ultra-long nanowires intertwined and assembled into a network structure of macroscopic self-standing MnO_2 architecture. After Ni or Co doping, the morphology of nanowires did not change distinctly. Thus, the Ni-MnO_2 and Co-MnO_2 also showed the disordered network structure assembled by nanowires.

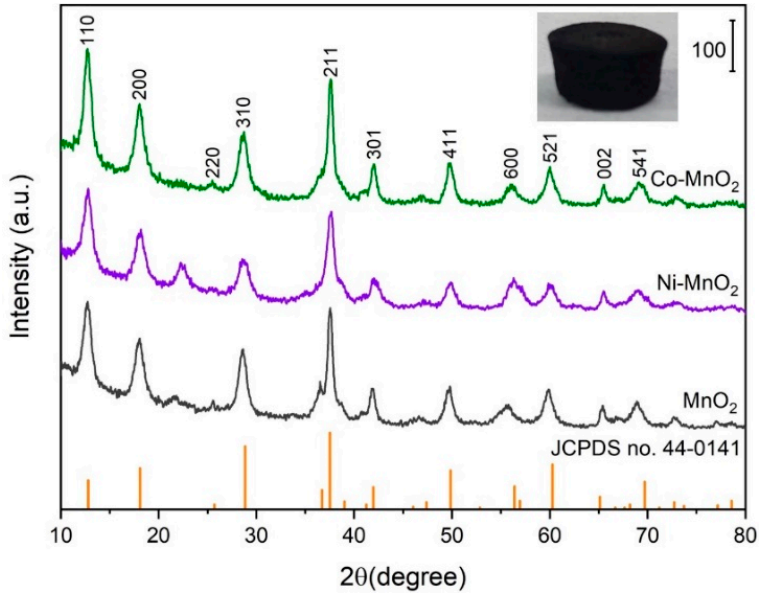

Figure 2. The X-ray diffractometer (XRD) patterns of pristine MnO_2, Ni-MnO_2, and Co-MnO_2 samples. The inset is the appearance of the macroscopic self-standing MnO_2 architecture.

On the basis of the aforesaid results, the fabrication process of macroscopic self-standing Mn-based architectures included the formation of wet gel with nanowires via hydrothermal reaction and the removal of water via ambient pressure drying maintaining the self-standing architecture simultaneously. In previous research, the MnO_2 short nanofibers were prepared and the wet gel was not formed without the addition of ammonium sulfate during the hydrothermal reaction [12,13]. The role of ammonium sulfate included: (1) modification of the nanostructure unit; the nanowires with large length-to-diameter ratio were obtained with the addition of ammonium sulfate and this morphology was favourable for the assembly, and (2) assistance to assembly; the ammonium sulfate functioned as bridging ligands and promoted the assembling of MnO_2 nanowires. It has been proposed that sulfate ions have two coordination sites which can bond water molecules via hydrogen bonds forming a three-dimensional network, and simultaneously coordinate metal nanoparticles, thus promoting nanoparticles self-assembly [14–16]. Therefore, the solvent of water also participated in the building process of the macroscopic assembly.

The mechanical properties of samples were investigated and the stress-strain curves were shown in Figure 4. The curves of all samples had a similar shape and contained elastic and plastic regions. The calculated Young's moduli in the linear region of pristine MnO_2, Ni-MnO_2, and Co-MnO_2 samples were 127, 73.8, and 172 MPa, suggesting they had good resistance to elastic deformation under load. The yield strengths of pristine MnO_2, Ni-MnO_2, and Co-MnO_2 samples reached 4.5, 3.2, and 4.2 MPa, respectively. In the plastic regions, when the samples were compressed to strain of 50%, the corresponding stresses of pristine MnO_2, Ni-MnO_2, and Co-MnO_2 samples were 6.2, 4.1, and 5.7

MPa. It suggested that all samples were robust, compared with manganese oxide sponges in previous research [10].

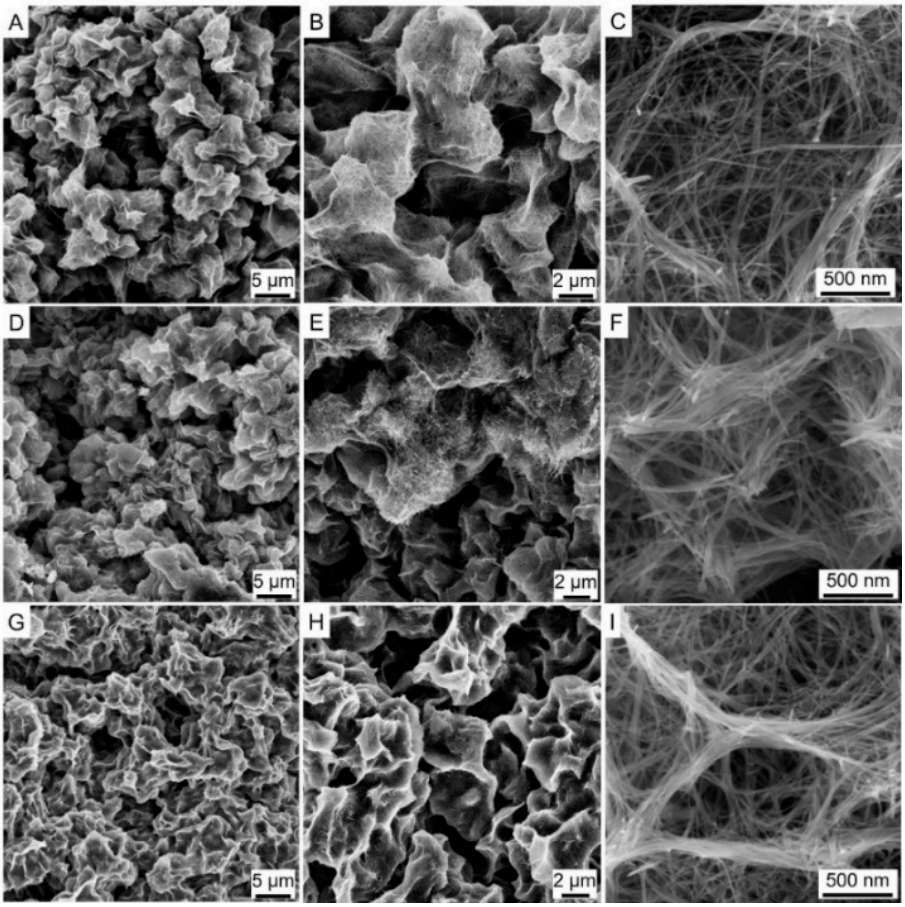

Figure 3. The Scanning Electron Microscopy (SEM) images of pristine MnO_2 (**A–C**), Ni-MnO_2 (**D–F**), and Co-MnO_2 (**G–I**) samples.

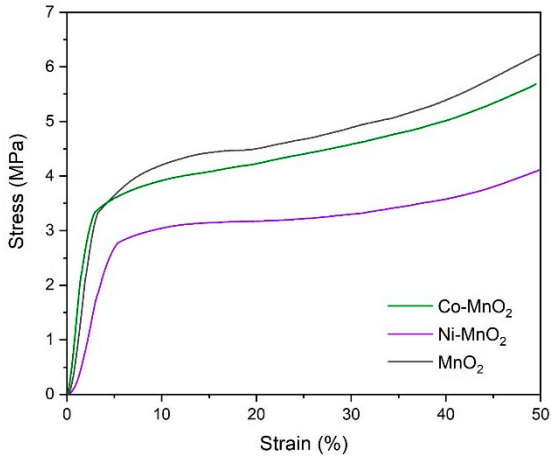

Figure 4. The mechanical properties of pristine MnO_2, Ni-MnO_2, and Co-MnO_2 samples.

The catalytic activities of propane oxidation over pristine MnO_2, Ni-MnO_2, and Co-MnO_2 samples were investigated and the results were shown in Figure 5. The T_{50} (the temperature at which 50% C_3H_8 was converted) was usually used to compare the performance of different samples. It was found that after incorporation of Ni or Co, the T_{50} shifted towards lower temperatures. Moreover, the T_{50} of Co-MnO_2 (278 °C) was lower than that of Ni-MnO_2 (289 °C), suggesting that Co-MnO_2 showed higher

activity for propane oxidation than Ni-MnO_2. When the temperature reached 400 °C, the conversion of propane over Co-MnO_2, Ni-MnO_2, and MnO_2 samples was 85.9, 84.3, and 58.6%, respectively. The results verified the promotional effect of Ni or Co doping on the catalytic activity for propane oxidation over MnO_2. After the reactions, the self-standing architectures did not deform or collapse, suggesting they had good resistance to thermal shock.

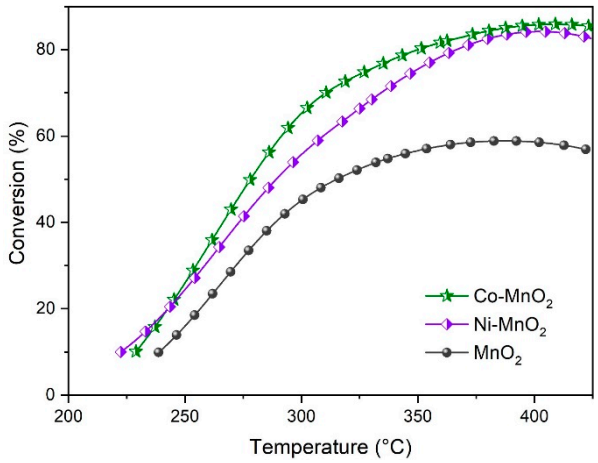

Figure 5. The catalytic activities for propane oxidation of pristine MnO_2, Ni-MnO_2 and Co-MnO_2 samples.

Furthermore, the turnover frequency (TOF) values were calculated to compare the catalytic activities of the three different catalysts. The detailed calculation method was described in previous research [17]. Based on the light-off curves and surface areas, the calculated results were shown in Table 1. It was found that the TOFs of samples increased in the order of MnO_2 (4.20×10^{-10} mol m^{-2} s^{-1}) < Ni-MnO_2 (4.53×10^{-10} mol m^{-2} s^{-1}) < Co-MnO_2 (5.10×10^{-10} mol m^{-2} s^{-1}), which suggested that the incorporation of Ni or Co remarkably enhanced the catalytic activity for propane oxidation.

Table 1. The surface areas and TOFs of the three catalysts.

	T_{10}	Surface Area (m^2 g^{-1})	TOF × 10^{10} (mol m^{-2} s^{-1})
MnO_2	239	70.8	4.20
Ni-MnO_2	223	67.8	4.53
Co-MnO_2	229	59.5	5.10

TOF = turnover frequency.

4. Conclusions

Macroscopic self-standing MnO_2 architecture was fabricated via hydrothermal reaction followed by ambient pressure drying. The addition of ammonium sulfate played an important role in the assembling of MnO_2 nanowires. After the Ni or Co doping, the macroscopic self-standing architectures could be maintained with excellent mechanical properties, which showed enhanced catalytic activities for propane oxidation. This study demonstrated a facile strategy to develop macroscopic self-standing Mn-based architectures, having great possibilities for practical applications.

Author Contributions: L.C. performed the experiments, analyzed the data and editted the paper; X.S. contributed review and supervision.

Funding: This research received no external funding.

Acknowledgments: We thank the ecomaterials laboratory of the School of Materials Science and Engineering, Tsinghua University, for performing the catalytic activity for propane oxidation tests.

Conflicts of Interest: The authors declare no conflict of interest.

References

1. Kim, S.C.; Shim, W.G. Catalytic combustion of VOCs over a series of manganese oxide catalysts. *Appl. Catal. B Environ.* **2010**, *98*, 180–185. [CrossRef]
2. Xie, Y.; Guo, Y.; Guo, Y.; Wang, L.; Zhan, W.; Wang, Y.; Gong, X.; Lu, G. A highly effective Ni-modified MnO_x catalyst for total oxidation of propane: The promotional role of nickel oxide. *Rsc. Adv.* **2016**, *6*, 50228–50237. [CrossRef]
3. Pahalagedara, L.; Kriz, D.A.; Wasalathanthri, N.; Weerakkody, C.; Meng, Y.; Dissanayake, S.; Pahalagedara, M.; Luo, Z.; Suib, S.L.; Nandi, P.; et al. Benchmarking of manganese oxide materials with CO oxidation as catalysts for low temperature selective oxidation. *Appl. Catal. B Environ.* **2017**, *204*, 411–420. [CrossRef]
4. Pahalagedara, L.R.; Dharmarathna, S.; King'ondu, C.K.; Pahalagedara, M.N.; Meng, Y.T.; Kuo, C.H.; Suib, S.L. Microwave-assisted hydrothermal synthesis of alpha-MnO_2: Lattice expansion via rapid temperature ramping and framework substitution. *J. Phy. Chem. C* **2014**, *118*, 20363–20373. [CrossRef]
5. Yang, J.; Zhou, H.; Wang, L.; Zhang, Y.; Chen, C.; Hu, H.; Li, G.; Zhang, Y.; Ma, Y.; Zhang, J. Cobalt-doped K-OMS-2 nanofibers: A novel and efficient water-tolerant catalyst for the oxidation of carbon monoxide. *ChemCatChem* **2017**, *9*, 1163–1167. [CrossRef]
6. Crespo-Biel, O.; Ravoo, B.J.; Reinhoudt, D.N.; Huskens, J. Noncovalent nanoarchitectures on surfaces: From 2D to 3D nanostructures. *J. Mater. Chem.* **2006**, *16*, 3997–4021. [CrossRef]
7. Shehzad, K.; Xu, Y.; Gao, C.; Duan, X. Three-dimensional macro-structures of two-dimensional nanomaterials. *Chem. Soc. Rev.* **2016**, *45*, 5541–5588. [CrossRef] [PubMed]
8. Long, Y.; Hui, J.F.; Wang, P.P.; Hu, S.; Xu, B.; Xiang, G.L.; Zhuang, J.; Lü, X.Q.; Wang, X. Alpha-MnO_2 nanowires as building blocks for the construction of 3D macro-assemblies. *Chem. Comm.* **2012**, *48*, 5925–5927. [CrossRef] [PubMed]
9. Jung, S.M.; Jung, H.Y.; Fang, W.; Dresselhaus, M.S.; Kong, J. A facile methodology for the production of in situ inorganic nanowire hydrogels/aerogels. *Nano Lett.* **2014**, *14*, 1810–1817. [CrossRef] [PubMed]
10. Liu, Z.; Wu, D.; Guo, X.; Fang, S.; Wang, L.; Xing, Y.; Suib, S.L. Robust macroscopic 3D sponges of manganese oxide molecular sieves. *Chem. Eur. J.* **2017**, *23*, 16213–16218. [CrossRef] [PubMed]
11. Rong, S.; Zhang, P.; Yang, Y.; Zhu, L.; Wang, J.; Liu, F. MnO_2 framework for instantaneous mineralization of carcinogenic airborne formaldehyde at room temperature. *ACS Catal.* **2017**, *7*, 1057–1067. [CrossRef]
12. Chen, L.; Ding, J.; Jia, J.; Ran, R.; Zhang, C.; Song, X. Cobalt-doped MnO_2 nanofibers for enhanced propane oxidation. *Acs Appl. Nano Mater.* **2019**, *2*, 4417–4426. [CrossRef]
13. Chen, L.; Ding, J.; Jia, J.; Ran, R.; Zhang, C.; Song, X. Nickel doping MnO_2 with abundant surface pits as highly efficient catalysts for propane deep oxidation. *Chem. Eng. J.* **2019**, *369*, 1129–1137. [CrossRef]
14. Fuchigami, T.; Kimata, R.; Haneda, M.; Kakimoto, K.I. Complex Three-dimensional Co_3O_4 nano-raspberry: Highly stable and active low-temperature CO oxidation catalyst. *Nanomaterials* **2018**, *8*, 662. [CrossRef] [PubMed]
15. Yao, F.; Chen, Y.G.; Salimi, A.R.; Mirzaei, M. Self-Assembly, Crystal structure and analysis of intermolecular interactions of the supramolecular compound based on hexamolybdochromate (III), sulfate and piperazine. *J. Clust. Sci.* **2011**, *22*, 309–318. [CrossRef]
16. Jeazet, H.B.T.; Gloe, K.; Doert, T.; Kataeva, O.N.; Jäger, A.; Geipel, G.; Bernhard, G.; Büchner, B.; Gloe, K. Self-assembly of neutral hexanuclear circular copper(II) meso-helicates: Topological control by sulfate ions. *Chem. Commun.* **2010**, *46*, 2373–2375. [CrossRef] [PubMed]
17. Hu, Z.; Qiu, S.; You, Y.; Guo, Y.; Guo, Y.; Wang, L.; Zhan, W.; Lu, G. Hydrothermal synthesis of $NiCeO_x$ nanosheets and its application to the total oxidation of propane. *Appl. Catal. B Environ.* **2018**, *225*, 110–120. [CrossRef]